

Response of circumnuclear water masers to luminosity changes in an active galactic nucleus

David A. Neufeld

Department of Physics & Astronomy, The Johns Hopkins University, 3400 North Charles Street,
Baltimore, MD 21218

ABSTRACT

Circumnuclear water masers can respond in two ways to changes in the luminosity of an active galactic nucleus. First, an increase in the X-ray luminosity can lead to an increase in the maser emissivity; and second, an increase in the intrinsic bolometric luminosity may result in a temporary *decrease* in the difference between the gas and dust temperature and a consequent *decrease* in the maser output. Whilst the latter effect can occur over a period shorter than the thermal timescale, the former effect cannot. Quantitative estimates of the response of the water maser emissivity to changes in either the X-ray or bolometric luminosity are presented, together with estimates of the relevant timescales. Either mechanism could account for recent observations by Gallimore et al. which suggest that the water maser variability in two widely separated regions of the circumnuclear gas in NGC 1068 have been coordinated by a signal from the active nucleus. For either mechanism, a minimum H_2 density $\sim 10^8 \text{ cm}^{-3}$ is needed to explain the observed variability timescale.

Subject headings: masers – galaxies: active – galaxies: individual: NGC 1068 – galaxies: nuclei – molecular processes – radio lines: galaxies

1. Introduction

Luminous maser emissions in the $6_{16} - 5_{23}$ 22 GHz line of water have now been detected from more than 20 active galaxies, a list of which is given in Table 2 of the recent review by Moran, Greenhill & Herrnstein (2000). In almost every case where the size of the emission region has been determined interferometrically, the water maser emission has been found to originate primarily within a parsec- or subparsec-sized region that is coincident with the active nucleus of the galaxy, suggesting that active galactic nuclei are the energy sources that ultimately power the observed water maser emission. In several sources, the geometry is strongly suggestive of a circumnuclear accretion disk (e.g. Miyoshi et al. 1995).

Theoretical models for the collisional excitation of water masers (e.g. de Jong 1973, Neufeld & Melnick 1991) place requirements on the physical conditions in the emitting region.

Luminous water maser emission is favored by molecular hydrogen densities, $n(\text{H}_2)$, in the range $10^7 - 10^{11} \text{cm}^{-3}$, water abundances, $x(\text{H}_2\text{O}) = n(\text{H}_2\text{O})/n(\text{H}_2) \gtrsim 10^{-4}$, and gas temperatures $\gtrsim 400 \text{ K}$. A minimum temperature requirement is imposed both by the excitation requirement for the maser transition and by the fact that water abundances are significantly enhanced at temperatures $\gtrsim 400 \text{ K}$ by the reaction $\text{O} + \text{H}_2 \rightarrow \text{OH} + \text{H}$ followed by $\text{OH} + \text{H}_2 \rightarrow \text{H}_2\text{O} + \text{H}$ (e.g. Elitzur & de Jong 1978; Neufeld, Lepp & Melnick 1995). An additional requirement is that the gas temperature must significantly exceed the temperature of the radiation field at mid- to far-infrared wavelengths: thus some energy source that directly heats the circumnuclear gas in active galaxies is needed to explain the observed water maser emission. X-rays from the active nucleus (Neufeld, Maloney & Conger 1994, hereafter NMC94), shock waves within a circumnuclear accretion disk (Maoz & McKee 1998), and viscous heating (Desch, Wallin & Watson 1998, hereafter DWW98) have all been proposed as the energy source responsible for heating the masing gas.

Detailed models for water masers in X-ray heated gas have been presented by NMC94, who considered the water maser emission as a function of depth into an X-irradiated slab. Those models showed that the physical and chemical conditions within X-ray heated gas are conducive to the excitation of water masers, and that – given reasonable assumptions about the nature of the circumnuclear emission region – X-ray heating could account for the typical luminosities of water masers observed in AGN. Collison and Watson (1995, hereafter CW95) subsequently made the important point that for certain parameters the maser emission can be significantly enhanced by the absorption of non-masing far-infrared water lines by dust, a process not included by NMC94.

Since AGN are known to exhibit significant and rapid variability (e.g. Ulrich, Maraschi, & Urry 1997) at optical, ultraviolet, and particularly X-ray wavelengths (e.g. Mushotzki, Done & Pounds 1993), maser models that invoke X-ray heating naturally raise the question of how the water maser emission would respond to changes in the incident X-ray and bolometric fluxes. This question, to be addressed this Letter, is also strongly motivated by observations of coordinated maser variability in NGC 1068 that have been reported recently by Gallimore et al. (2000). In §2 below, I present the results of a general parameter study for the equilibrium maser emission from a warm dusty medium. In §3, I consider how the maser emission responds to changes in the illuminating X-ray flux or in the dust temperature within the masing medium. In §4, the results are discussed with specific reference to the water masers in NGC 1068.

2. Water maser emission from a warm dusty medium

The collisional excitation of water masers within a warm dusty medium has been modeled by Wallin & Watson (1997) in the limit where the medium is optically thick to far-infrared continuum radiation. As previously pointed out by CW95, this limit often applies to circumnuclear gas in AGN, given the continuum dust opacities typically present (Draine & Laor 1993). The effect of continuum opacity is to place a lower limit on the escape probability for non-masing far-infrared transitions of water, allowing maser emission to occur even at great depths within a circumnuclear

disk or gas cloud and enhancing the cooling rate due to far-infrared water emissions (DWW98).

In the limit where the medium is optically thick to far-infrared continuum radiation, the water level populations are determined solely by the local conditions and are dependent on the gas temperature, T_{gas} , the dust temperature, T_{dust} , the H_2 density, $n(\text{H}_2)$, and the water abundance $x(\text{H}_2\text{O}) = n(\text{H}_2\text{O})/n(\text{H}_2)$. Since water abundances $\sim 10^{-4}$ are predicted for regions of luminous water maser emission, I have constructed a grid of models for fixed $x(\text{H}_2\text{O}) \sim 10^{-4}$ that span a broad region in the three dimensional parameter space defined by T_{gas} , T_{dust} , and $n(\text{H}_2)$.

The water level populations are given by the usual equations of statistical equilibrium (e.g. CW95), with the rates for all radiative processes diminished by an escape probability $\beta_{ij}^c = [2\alpha_{ij}/(1+2\alpha_{ij})](\ln[e + \pi^{-1/2}\alpha_{ij}^{-1}])^{1/2}$, where α_{ij} is the ratio of dust continuum opacity to line center opacity for the transition from i to j (Hollenbach & McKee 1979, CW95). For consistency with the previous work of CW95, we assume a continuum absorption coefficient of $10^{-23}n_{\text{H}}\text{cm}^2$ for wavelengths $\lambda \leq 50\mu\text{m}$ and $10^{-23}n_{\text{H}}(50\mu\text{m}/\lambda)^2\text{cm}^2$ for $\lambda \geq 50\mu\text{m}$, where n_{H} is the density of H nuclei. For comparison, the probability of escape from a semi-infinite plane parallel slab is $\beta_{ij} = (4\pi^{1/2}\tau_{ij}[\ln\tau_{ij}]^{1/2})^{-1}$ in the limit where the line center optical depth $\tau_{ij} \gg 1$ (Hollenbach & McKee 1979). Comparing these expressions, we find that dust absorption dominates the effective escape of far-infrared water emissions for dust optical depths $\geq (8\pi^{1/2})^{-1} = 0.07$, corresponding to column densities of H nuclei, $N_{\text{H}} \gtrsim 10^{22}\text{cm}^{-2}$. Following Neufeld & Kaufman (1993, hereafter NK93), I solved the equations of statistical equilibrium for 179 rotational states of ortho-water, adopting the collisional rate coefficients of Green, Maluendes & McLean (1993) for transitions among the lowest 45 states and a simple extrapolation for transitions involving states of higher energy. The assumed line width, defined as velocity shift needed to reduce the opacity from its peak value by a factor e , was 1 km s^{-1} .

Once the statistical equilibrium equations have been solved, the cooling rate due to water emissions and the rate of maser emission under conditions of saturation may be obtained straightforwardly (e.g. Neufeld & Melnick 1991; NK93). The results I obtained for the maser emissivity are in good agreement with those presented previously by Wallin & Watson (1997). If the gas is in thermal equilibrium, then the required heating rate is equal to the cooling rate, which – for the conditions of relevance here – is dominated by water cooling and gas-grain collisional cooling (Neufeld et al. 1995). Using the gas-grain cooling rate adopted by DWW98 and the water cooling rate obtained above, I computed the equilibrium heating rate, H , and used it in place of T_{gas} as one of the three dependent variables.

Figure 1a shows a contour plot of the gas temperature, T_{gas} , and the maser efficiency, $\epsilon_{\text{sat}}^0 = h\nu\Phi_{\text{sat}}^0/(n_{\text{H}}H)$, as function of T_{dust} and H/n_{H} . Here Φ_{sat}^0 is the rate at which maser photons are emitted per unit volume, the superscript 0 indicating that the results apply to the case where the dust optical depth is large (Watson & Wallin 1997) and the subscript sat indicating that the maser emission is assumed to be saturated. The heating rate, H , is defined following the notation of Maloney, Hollenbach & Tielens (1996, hereafter MHT96) as the heating rate per hydrogen

nucleus (with units erg s^{-1}). The maser efficiency ϵ_{sat}^0 is thus the fraction of the input power that emerges as 22 GHz maser radiation. The results shown in Figure 1a apply to a fixed molecular hydrogen density $n(\text{H}_2) = \frac{1}{2}n_{\text{H}} = 10^9 \text{ cm}^{-3}$.

As required by the second law of thermodynamics, Figure 1 shows that $T_{\text{gas}} \rightarrow T_{\text{dust}}$ in the limit $H \rightarrow 0$. There is a minimum value of the heating rate (defined by the curve $\epsilon_{\text{sat}}^0 = 0$) below which $T_{\text{gas}} - T_{\text{dust}}$ is insufficient to support a population inversion. The vertical line at $H/n_{\text{H}} \sim 1.2 \times 10^{-28} \text{ erg cm}^3 \text{ s}^{-1}$ represents the *maximum* X-ray heating rate that can be sustained without the gas being dissociated (NMC94). Thus the region for luminous maser action within an X-ray heated medium lies to the right of the curve $\epsilon_{\text{sat}}^0 = 0$, to the left of the line $H/n_{\text{H}} = 1.2 \times 10^{-28} \text{ erg cm}^3 \text{ s}^{-1}$, and above the curve $T_{\text{gas}} = 400 \text{ K}$ (the latter requirement being needed for consistency with the large water abundance of 10^{-4} that has been assumed). Figure 1b presents analogous results to those in Figure 1a, but now ϵ_{sat}^0 and T_{gas} are shown for a fixed dust temperature (500 K) as a function of $n(\text{H}_2)$ and H/n_{H} .

3. Response of masers to a change in their environment

Results shown in Figure 1 apply to conditions of thermal equilibrium. The effects of changing the heating rate and dust temperature can now be considered. The timescale for the gas to re-establish thermal equilibrium after a change in the heating rate or dust temperature is given by $\tau_{\text{therm}} = \frac{5}{2}kT/2H = 0.027 (T/1000 \text{ K}) (n(\text{H}_2)/10^9 \text{ cm}^{-3})^{-1} ([H/n_{\text{H}}]/10^{-28} \text{ erg cm}^3 \text{ s}^{-1})^{-1} \text{ yr}$. Let us first consider the effects of changing the heating rate. On timescales greater than τ_{therm} , an increase in the heating rate increases the difference between the gas and dust temperatures and increases the rate of maser emission. The response is then conveniently characterized by the logarithmic derivative $\partial \ln \Phi_{\text{sat}}^0 / \partial \ln H = 1 + (\partial \ln \epsilon_{\text{sat}}^0 / \partial \ln H)$, which is plotted in Figure 2 (dashed curve) for $n(\text{H}_2) = 10^9 \text{ cm}^{-3}$ and $T_{\text{dust}} = 500 \text{ K}$. Except for small values of H close to the threshold for maser action, the derivative $\partial \ln \Phi_{\text{sat}}^0 / \partial \ln H$ lies within a factor of 2 of unity, implying that changes in the heating rate are accompanied by comparable fractional changes in the maser emission rate.

The results plotted in Figure 2 are premised on assumptions of constant density and water abundance. The density is only expected to change on a dynamical timescale, which is typically much longer than τ_{therm} . The molecular fraction, $2n(\text{H}_2)/n_{\text{H}}$, only changes on the X-ray ionization timescale, which is given (MHT96) by $\sim 4 (n(\text{H}_2)/10^9 \text{ cm}^{-3})^{-1} ([H/n_{\text{H}}]/10^{-28} \text{ erg cm}^3 \text{ s}^{-1})^{-1} \text{ yr}$ and is a factor ~ 200 greater than the cooling timescale. Even if the molecular fraction is constant, however, the water abundance can change in response to changes in the temperature. This effect, the inclusion of which lies beyond the scope of the present study, is unlikely to be important except when the gas temperature lies close to the threshold for rapid water production ($T_{\text{gas}} \sim 400 \text{ K}$) or when the X-ray ionization rate lies close to the threshold for molecular dissociation.

If the heating rate varies, the gas temperature and maser emissivity Φ_{sat}^0 cannot

respond on timescales any shorter than τ_{therm} . However, Φ_{sat}^0 *can* vary on timescales shorter than τ_{therm} if the dust temperature changes rapidly. The thermal inertia of the dust grains is negligible, so the timescale on which the dust temperature can change is controlled by the diffusion time for the far-infrared continuum radiation¹, given by $\tau_{\text{rad}} \sim \tau_{\text{FIR}} \ell / c \sim 0.005 [N_H / 10^{24} \text{ cm}^{-2}]^2 [n(\text{H}_2) / 10^9 \text{ cm}^{-3}]^{-1} \text{ yr}$, where ℓ is the distance below the irradiated surface of the cloud and $\tau_{\text{FIR}} \sim 10 (N_H / 10^{24} \text{ cm}^{-3})$ (assumed ≥ 1) is the corresponding optical depth at far-infrared wavelengths.

Under circumstances where the dust temperature varies on timescales shorter than τ_{therm} – as it might in response to variations in the incident bolometric flux from the AGN, for example – the gas temperature remains constant but the maser emissivity varies as a result of changes in the difference between the gas and dust temperatures, $T_{\text{diff}} = T_{\text{gas}} - T_{\text{dust}}$. The response is now characterized by the derivative $(\partial \ln \Phi_{\text{sat}}^0 / \partial \ln T_{\text{dust}})_{T_{\text{gas}}}$, the subscript T_{gas} indicating that the gas temperature is held constant. The dotted curve in Figure 2 shows the value of this derivative, again for the case where $n(\text{H}_2) = 10^9 \text{ cm}^{-3}$ and $T_{\text{dust}} = 500 \text{ K}$. Two features of this curve are particularly noteworthy. First, the value of $(\partial \ln \Phi_{\text{sat}}^0 / \partial \ln T_{\text{dust}})_{T_{\text{gas}}}$ is always negative because T_{diff} decreases as T_{dust} increases. Second, $(\partial \ln \Phi_{\text{sat}}^0 / \partial \ln T_{\text{dust}})_{T_{\text{gas}}}$ can become much larger than unity for small values of H . This behavior occurs because the maser emissivity is primarily controlled by T_{diff} ; a small fractional change in T_{dust} causes a large fractional change in T_{diff} when $T_{\text{diff}} \ll T_{\text{dust}}$.

4. Application to NGC 1068

The results presented in Figures 1 and 2 can now be discussed with reference to recent observations of the Seyfert galaxy NGC 1068. Gallimore et al. (2000) have recently reported that two maser features in NGC 1068, symmetrically placed in Doppler velocity about the systemic velocity of the host galaxy, flared simultaneously with a rise time of at most 22 days. Given the emission region structure elucidated by earlier VLBA observations (Greenhill & Gwinn 1997), the velocities of the maser features involved suggest that they are symmetrically located at distance $d \sim 0.7 \text{ pc}$ on either side of the nucleus. Unless the simultaneity of the flares is entirely happenstance, they were presumably coordinated by a signal that propagated from the nucleus.

The results presented in Figure 2 suggest two possible mechanisms for how the maser flares might be coordinated: (1) variations in the central X-ray luminosity, L_X , might simultaneously change the heating rates in the masing regions; or (2) variations in the intrinsic bolometric luminosity, L_{bol} , might simultaneously change the dust temperature². Unfortunately, the average

¹This is the shortest timescale on which the *local* infrared radiation field can vary; note that the infrared flux *as viewed from afar* may have a characteristic variability timescale that is considerably longer than that of the local infrared radiation as a result of the different light travel times from the near and far sides of the irradiated disk or torus.

²For the case of saturated masers, an third mechanism is possible: in principle, the observed flares might be

X-ray and bolometric luminosities are rather uncertain for NGC 1068, since the central source is obscured even for hard X-rays; I adopted the estimates of Pier et al. (1994), who compiled observations obtained over a wide range of wavelengths and assumed that 1% of the total intrinsic luminosity is reflected towards us. These estimates of the luminosities imply a 1 – 100 keV X-ray flux $\sim 7 \times 10^5 \text{ erg cm}^{-2} \text{ s}^{-1}$ at the distance of the flaring masers and a characteristic dust temperature $\sim (L_{\text{bol}}/4\pi d^2 \sigma)^{1/4} \sim 500 \text{ K}$. Expressions given by MHT96 then imply an X-ray heating rate $H \sim 5.6 \times 10^{-20} (N_{\text{H}}/10^{24} \text{ cm}^{-2})^{-0.9} \text{ erg s}^{-1}$ at column density N_{H} below the irradiated surface of the maser emission region. For column densities greater than $N_{\text{H}} \sim 10^{24} \text{ cm}^{-2}$, Thomson scattering becomes important and increases the effective column density appearing in the above equation for H by a factor $\sim \tau_T = 6.65 \times 10^{-25} N_{\text{H}} \text{ cm}^2$.

In Figure 3, relevant constraints are plotted³ as a function of $n(\text{H}_2)$ and N_{H} . Molecules are present above and to the right of the line $H/n_{\text{H}} = 1.2 \times 10^{-28} \text{ erg cm}^3 \text{ s}^{-1}$. Maser action can occur below and to the left of the curve $\epsilon_{\text{sat}}^0 = 0$. The observed variability can be driven by changes in the X-ray heating rate for parameters to the left of the line $\tau_{\text{therm}} = 0.05 \text{ yr}$; or alternatively by changes in the dust temperature for the region to the left of the line $\tau_{\text{rad}} = 0.05 \text{ yr}$ and to the right of the line $\tau_{\text{therm}} = 0.05 \text{ yr}$. In either case, the minimum required H_2 density for a variability timescale of 0.05 yr is $\sim 10^8 \text{ cm}^{-2}$. In Figure 4, the derivatives $\partial \ln \Phi_{\text{sat}}^0 / \partial \ln L_X$ and $(\partial \ln \Phi_{\text{sat}}^0 / \partial \ln L_{\text{bol}})_{T_{\text{gas}}}$ are shown for several values of the density. Since the dust temperature increases as $L_{\text{bol}}^{1/4}$, the latter derivative is given by $\frac{1}{4}(\partial \ln \Phi_{\text{sat}}^0 / \partial \ln T_{\text{dust}})_{T_{\text{gas}}}$.

Figures 3 and 4 indicate that the simultaneous flaring of the two maser features in NGC 1068 could plausibly be coordinated *either* through variations in the heating rate *or* through variations in the dust temperature. The former mechanism would be unique to X-ray heating whereas the latter might apply in principle even if shock heating or viscous heating were responsible for the maser emission. Observationally, the mechanisms might be discriminated by searching for correlations between the maser emission and X-ray and bolometric luminosities, although in the case of NGC 1068 the fact that we observe only reflected radiation from the nucleus will introduce uncertain delays that will be difficult to remove. Maser variability induced by a varying X-ray heating rate will be characterized by a positive correlation with L_X (with a time delay determined by the different light travel times, of course), while variability induced by a varying

coordinated by a varying 22 GHz continuum flux from a compact central source. Since the maser radiation from the flaring regions travels tangentially toward us, the flux we receive from those regions might increase if the radial flux of seed radiation from the central source diminished. This explanation, however, would require that the maser emission is controlled by seed radiation from a compact continuum source; in NGC 1068 the observed distribution of maser emission close to the systemic velocity argues against that being the case.

³The results plotted here apply to a gas cloud that is illuminated at normal incidence such that the column densities for X-ray shielding and for the escape of far-infrared radiation are identical. For oblique illumination at angle θ to the normal, the column density N_{H} refers to the shielding column density, the timescale τ_{rad} is reduced by a factor $\sec^2 \theta$, and the dust temperature should be reduced by a factor $(\sec \theta)^{1/4}$. An additional assumption is that dust absorption dominates the removal of far-infrared line photons, requiring $N_{\text{H}} \cos \theta \gtrsim 10^{22} \text{ cm}^{-2}$.

dust temperature will be characterized by a negative correlation with L_{bol} .

It is a pleasure to acknowledge helpful discussions with E. Agol and J. Gallimore. I gratefully acknowledge the support of a National Young Investigator award from the National Science Foundation.

REFERENCES

- Collison, A. J. and Watson, W. D. 1995, ApJ, 452, L103 (CW95)
- de Jong, T. 1973, A&A, 26, 297
- Desch, S. J., Wallin, B. K. and Watson, W. D. 1998, ApJ, 496, 775
- Elitzur, M. and de Jong, T. 1978, A&A, 67, 323
- Gallimore, J.F., Baum, S.A., Henkel, C., Glass, I.S., Claussen, M.J., Almudena Prieto, M., & von Kap-herr, A. 2000, ApJ, submitted
- Green, S., Maluendes, S. and McLean, A. D. 1993, ApJS, 85, 181
- Greenhill, L. J. and Gwinn, C. R. 1997, Ap&SS, 248, 261
- Hollenbach, D. and McKee, C. F. 1979, ApJS, 41, 555
- Laor, A. and Draine, B. T. 1993, ApJ, 402, 441
- Maloney, P. R., Hollenbach, D. J. and Tielens, A. G. G. M. 1996, ApJ, 466, 561 (MHT96)
- Maoz, E. and McKee, C. F. 1998, ApJ, 494, 218
- Moran, J.M., Greenhill, L.J., and Herrnstein, J.R. 2000, to appear in *Proceedings of the Discussion Meeting on the Physics of Black Holes* (Bangalore, India: December 8 – 10, 1997). Special issue of the Journal of Astrophysics and Astronomy.
- Miyoshi, M., Moran, J., Herrnstein, J., Greenhill, L., Nakai, N., Diamond, P. and Inoue, M. 1995, Nature, 373, 127
- Mushotzky, R. F., Done, C. and Pounds, K. A. 1993, ARA&A, 31, 717
- Neufeld, D. A. and Melnick, G. J. 1991, ApJ, 368, 215 (Erratum: 374, 784)
- Neufeld, D. A. and Kaufman, M. J. 1993, ApJ, 418, 263 (NK93)
- Neufeld, D. A., Maloney, P. R. and Conger, S. 1994, ApJ, 436, L127 (NMC94)
- Neufeld, D. A., Lepp, S. and Melnick, G. J. 1995, ApJS, 100, 132

Pier, E. A., Antonucci, R., Hurt, T., Kriss, G. and Krolik, J. 1994, ApJ, 428, 124

Ulrich, M., Maraschi, L. and Urry, C. M. 1997, ARA&A, 35, 445

Wallin, B. K. and Watson, W. D. 1997, ApJ, 481, 832

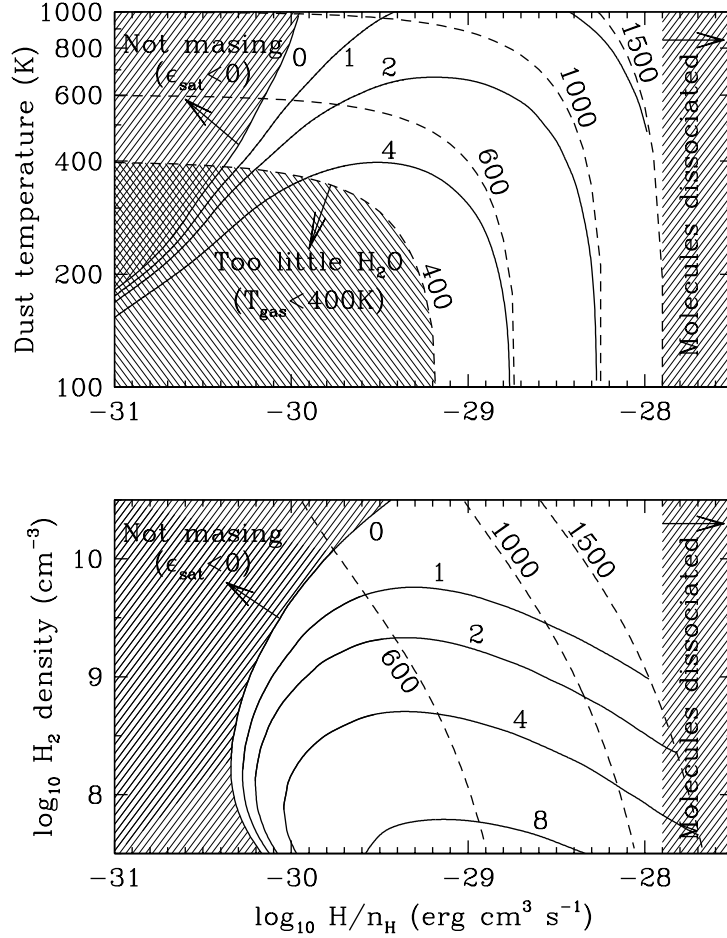


Fig. 1.— Maser efficiency (solid contours labeled with $10^5 \times \epsilon_{\text{sat}}^0$) and gas temperature (dashed contours labeled with T_{gas} in K). Results are shown as a function of heating rate, H , and either dust temperature (Figure 1a, top panel, for which the H₂ density is fixed at 10^9 cm⁻³) or H₂ density (Figure 1b, bottom panel, for which the dust temperature is fixed at 500 K). The assumed water abundance for both panels is 10^{-4} relative to H₂. The region favorable to efficient maser emission is the unshaded region where the gas temperature is large enough ($\gtrsim 400$ K) to yield a substantial water abundance and where the heating rate supports a value of $(T_{\text{gas}} - T_{\text{dust}})$ large enough to permit maser action but is not so large as to dissociate molecules.

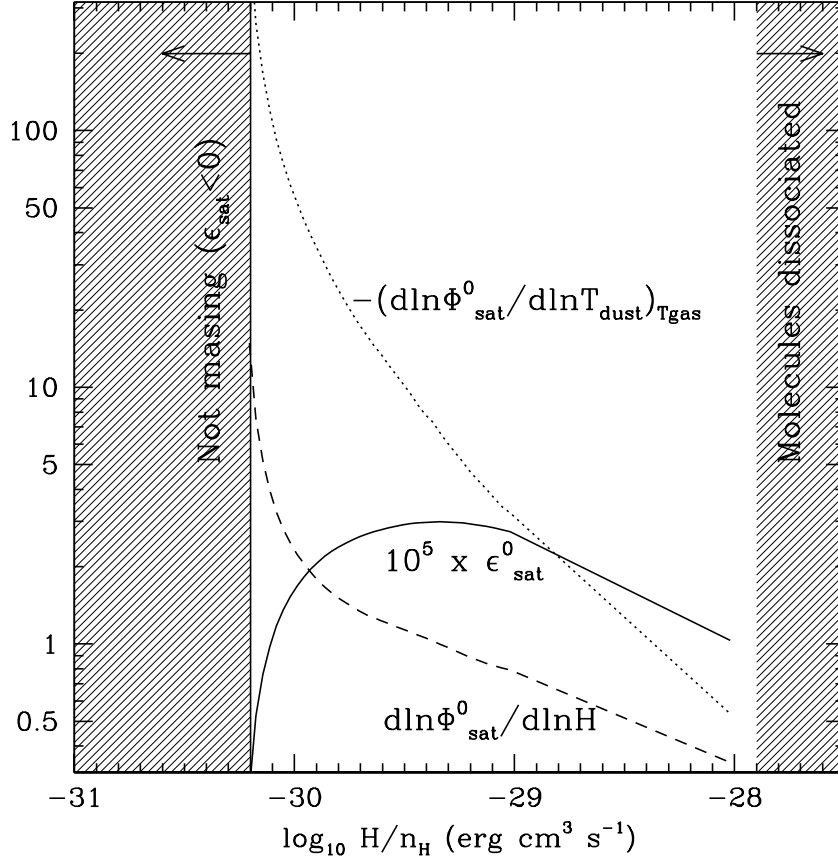


Fig. 2.— Response of maser emissivity to small changes in the heating rate and dust temperature, for a dust temperature of 500 K and a H_2 density of 10^9 cm^{-3} . Values of the derivatives $\partial \ln \Phi_{\text{sat}}^0 / \partial \ln H$ (dashed curve) and $(\partial \ln \Phi_{\text{sat}}^0 / \partial \ln T_{\text{dust}})_{T_{\text{gas}}}$ (dotted curve) are shown as a function of the heating rate, H (see text). The solid curve shows the maser emissivity (value plotted is $10^5 \times \epsilon_{\text{sat}}^0$.)

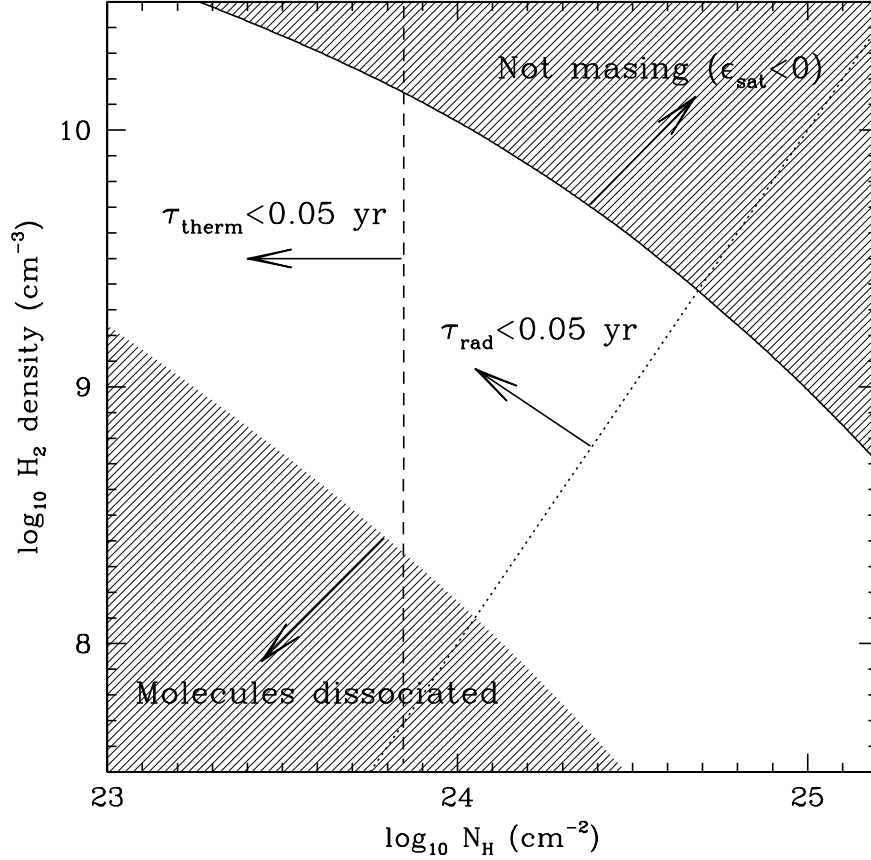


Fig. 3.— Parameter space for maser action and variability in clouds 0.7 pc distant from the active nucleus of NGC 1068. Results are shown as a function of the H_2 density and the column density for X-ray shielding. Regions of parameter space for which there is no maser emission are shaded. The dashed line shows where the thermal timescale for the gas is 0.05 yr, and the dotted line shows where the radiative diffusion timescale governing changes in the dust temperature is 0.05 yr. The coordinated maser variability reported by Gallimore et al. (2000) can be driven by changes in the X-ray heating rate for parameters to the left of the line $\tau_{\text{therm}} = 0.05 \text{ yr}$; or alternatively by changes in the dust temperature for the region to the left of the line $\tau_{\text{rad}} = 0.05 \text{ yr}$ and to the right of the line $\tau_{\text{therm}} = 0.05 \text{ yr}$.

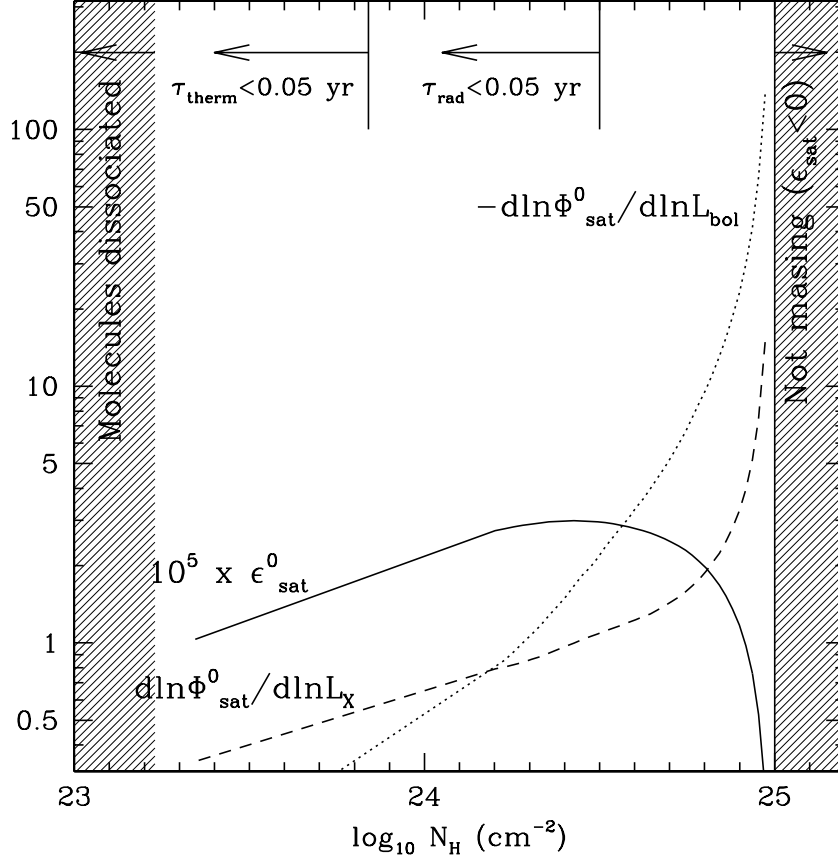


Fig. 4.— Same as Figure 2, but now plotted as a function of the column density for X-ray shielding. Results apply to a cloud of H_2 density 10^9 cm^{-3} that is 0.7 pc distant from the active nucleus of NGC 1068. Arrows indicate the range of column densities for which the thermal timescale for the gas and the radiative diffusion timescale governing changes in the dust temperature are smaller than 0.05 yr.